Shpotyuk et al. Nanoscale Research Letters (2016) 11:20
DOI 10.1186/s11671-016-1237-8

Nanoscale Research Letters
a SpringerOpen Journal

NANO EXPRESS Open Access

Free-Volume Nanostructurization in Ga-Modified As_2Se_3 Glass

Ya. Shpotyuk[1,2,3*], A. Ingram[4], O. Shpotyuk[5,6], A. Dziedzic[2], C. Boussard-Pledel[3] and B. Bureau[3]

Abstract

Different stages of intrinsic nanostructurization related to evolution of free-volume voids, including phase separation, crystalline nuclei precipitation, and growth, were studied in glassy As_2Se_3 doped with Ga up to 5 at. %, using complementary techniques of positron annihilation lifetime spectroscopy, X-ray powder diffraction, and scanning electron microscopy with energy-dispersive X-ray analysis. Positron lifetime spectra reconstructed in terms of a two-state trapping model testified in favor of a native void structure of g-As_2Se_3 modified by Ga additions. Under small Ga content (below 3 at. %), the positron trapping in glassy alloys was dominated by voids associated with bond-free solid angles of bridging $As_2Se_{4/2}$ units. This void agglomeration trend was changed on fragmentation with further Ga doping due to crystalline Ga_2Se_3 nuclei precipitation and growth, these changes being activated by employing free volume from just attached As-rich glassy matrix with higher content of $As_2Se_{4/2}$ clusters. Respectively, the positron trapping on free-volume voids related to pyramidal $AsSe_{3/2}$ units (like in parent As_2Se_3 glass) was in obvious preference in such glassy crystalline alloys.

Keywords: Chalcogenides, Nanostructurization, Phase separation, Crystallization, Positron annihilation lifetime spectroscopy

Background

Ga-modified chalcogenide glasses (ChG) are known to be of high importance in view of their perspectives for modern IR photonics as active media with improved optical functionality, revealed, in part, when these glasses are doped with rare earth (RE) activators such as Pr^{3+}, Dy^{3+}, Tb^{3+}, Er^{3+}, and Nd^{3+} [1–9]. Such ChG demonstrates an obvious tendency to nanostructurization by forming intrinsic inhomogeneities because of strong Ga affinity to chemical interaction with chalcogens, this process being governed by Ga content and preferential type of its environment in parent glass matrix [4, 10–16]. In dependence on these pre-requisites, extra Ga additions can result in phase separation, nucleation and, finally, crystal growth, leading to stabilization of different crystalline Ga_2Se_3 polymorphs. Thus, under small Ga content (2–3 at. %) added in mixed Se–Te environment of TAS-235 glass (e.g., glassy g-$As_{30}Se_{50}Te_{20}$ alloy), the nanoscale droplets of dominated γ-Ga_2Se_3 phase (a few hundreds of nanometers in sizes) can be displayed, while at more enhanced Ga content reaching 5–10 at. %, this process extends over a microscale, when these crystallites grow to a few micrometers in sizes [8, 13]. In contrast, in Se-rich environment of Ge-based $GeSe_2$–Ga_2Se_3 glass at heat treatment not too far above T_g, these Ga additions provoke formation of some multication crystallites like $GeGa_4Se_8$ [14–16] or $Ga_{2-\delta}Ge_\delta Se_3$ [12]. Crystallite growth and stabilization in ChG matrices is accompanied by complicated changes stretching over both atomistic (atomic-specific) and void (atomic-deficient) structural levels. The latter is related to the evolution of some free-volume entities (typically sub-nanoscale voids, vacancies, vacancy-like clusters, etc.), when inner holes are agglomerated to form spaces of reduced electron density available for orientation stabilization of growing crystallites or, conversely, these holes are fragmented on smaller parts ensuring energetically favorable localization for growing crystallites in a predominantly glass environment [13]. In case of technologically controlled crystallization, it is possible to manufacture an important class of glass ceramics transparent in IR region, which possess much better mechanical reliability than their glassy counterparts [17]. But in most cases, these crystallization processes are

* Correspondence: yashpotyuk@gmail.com
[1]Department of Electronics, Ivan Franko National University of Lviv, 107, Tarnavskogo str., 79017 Lviv, Ukraine
[2]Centre for Innovation and Transfer of Natural Sciences and Engineering Knowledge, University of Rzeszow, 1, Pigonia str., 35-959 Rzeszow, Poland
Full list of author information is available at the end of the article

undesirable, especially when ChG should be doped with RE ions to get tunable, high-power, secondary remote mid-IR sources [9], or drawn into fiber to produce active media for optical biosensing [18].

In this work, the physical peculiarities of Ga-affected nanostructurization associated with subsequent stages of glass structure modification (phase separation, nucleation, and crystallization), overall described at atomic-deficient void level, are comprehensively studied in g-As_2Se_3, one of the well-known canonical representatives of functional chalcogenide photonics [19].

Methods

The studied samples of $Ga_x(As_{0.4}Se_{0.6})_{100-x}$ (x = 0, 1, 2, 3, 4, 5) alloys were prepared from high-purity elemental constituents (5 N or more) by conventional melt-quenching technique as described elsewhere [9, 11]. Total weight of ingredients inserted in silica ampoules of 10 mm in diameter used for melting was 30 g. The ampoule was sealed under a vacuum and heated at 900 °C in a rocking furnace for 10 h, followed by quenching into room temperature water from 700 °C. Then, these alloys were annealed during 5 h at 10 K below glass transition to remove mechanical strains that appeared during quenching, cut into disks of ~2 mm in thickness, and finally, polished to high optical quality.

The crystalline state of the samples was controlled with X-ray powder diffraction (XRPD), experimental data being collected in the transmission mode on a STOE STADI P diffractometer (Cu $K\alpha_1$-radiation). The crystal structures of phases were refined by the Rietveld method with the program FullProf.2k (v. 5.40) [20]. The surface morphology of fresh cut sections of the prepared alloys was tested using scanning electron microscope (SEM) with energy-dispersive spectroscopy (EDS) analyzer FEI QUANTA 3D 200i (Hillsboro, OR, USA).

Positron annihilation lifetime (PAL) spectra were registered using fast coincidence system ORTEC of 230 ps resolution (the full width at half maximum) operated at high-stabilized normal measuring conditions. The pair of identical plane-parallel samples of each composition in sandwich geometry was employed for the measurements. The source contribution from ^{22}Na isotope of low activity was taken at the level of 12 % (τ = 0.372 ns). To ensure reliable PAL data, three independent measuring cycles (with near 1 M elementary positron annihilation events) were performed. Experimental results were fitted by two single exponents under normalized intensities ($I_1 + I_2 = 1$) using LT 9.0 program [21], the corresponding accuracies in lifetimes τ_i and intensities I_i being not worse ±0.005 ns and 0.5 %, respectively. Mathematical formalism of the known two-state positron trapping model with only one kind of traps [22–26] was utilized to parameterize mean τ_{av} and defect-free bulk τ_b lifetimes, as well as trapping rate in defects κ_d. In addition, the difference between defect-related $\tau_d = \tau_2$ and bulk positron lifetimes ($\tau_2 - \tau_b$) was taken as a signature of size of positron traps in terms of equivalent number of vacancies, and τ_2/τ_b ratio was ascribed to nature of these defects [22]. The fraction of trapped positrons $\eta = \tau_1 \cdot \kappa_d$ was also controlled in this research.

Results and Discussion

Different stages of intrinsic nanostructurization can be activated in g-As_2Se_3 in dependence on the amount of added Ga [9, 11]. Firstly, at small enough Ga content within studied $Ga_x(As_{0.4}Se_{0.6})_{100-x}$ cut section not exceeding 3 at. %, the melt-quenched alloys are fully in a glassy state, since no any sharp reflexes (but only wide-stretched halos typical for amorphous substances) are detected on the XRPD patterns [9]. Further, at higher Ga content, some crystallites of low-temperature α-Ga_2Se_3 phase appear in glassy crystalline g/c-$Ga_4(As_{0.4}Se_{0.6})_{96}$ alloy, the crystallized phase being well identified due to six sharp XRPD peaks corresponding to one of cubic Ga_2Se_3 polymorphs with a space group of $F\bar{4}3m$ (JCPDS ICDD card no. 89-7201) [9, 27–29]. The most pronounced crystallization effect is revealed in g/c-$Ga_5(As_{0.4}Se_{0.6})_{95}$, where ten separate XRPD peaks centered near 28.5°, 33°, 47°, 56°, 69°, 76°, 87.5°, 94.5°, 106°, and 113° 2Θ are detected (Fig. 1). These peaks can be well indexed assuming *fcc* Ga_2Se_3 structure of zinc blende type ($F\bar{4}3m$ space group), which allow to estimate the unit cell lattice parameter a = 5.4576(6) Å (with respective unit cell volume V = 162.55(3) $Å^3$). In accord with similar behavior in Ga-doped g-$As_{30}Se_{50}Te_{20}$ [8, 13], this effect can be ascribed to preferential formation of high-temperature γ-Ga_2Se_3 phase.

Under this Ga content, the crystallization is most evident, the cones of four to six separate Ga_2Se_3 crystallites

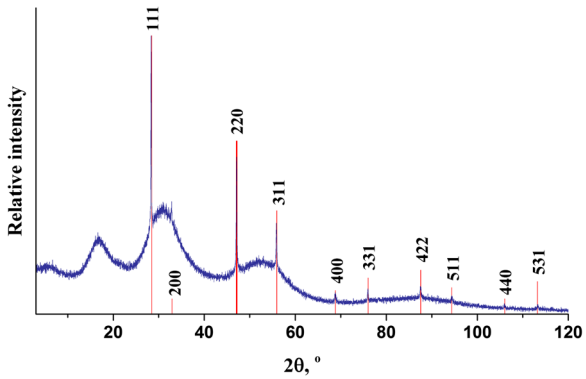

Fig. 1 Experimental XRPD pattern of g/c-$Ga_5(As_{0.4}Se_{0.6})_{95}$ sample (*blue color*) in comparison with theoretical diffraction pattern of Ga_2Se_3 high-temperature phase of ZnS structural type. (*red color*, *hkl* indexes are indicated above the peaks)

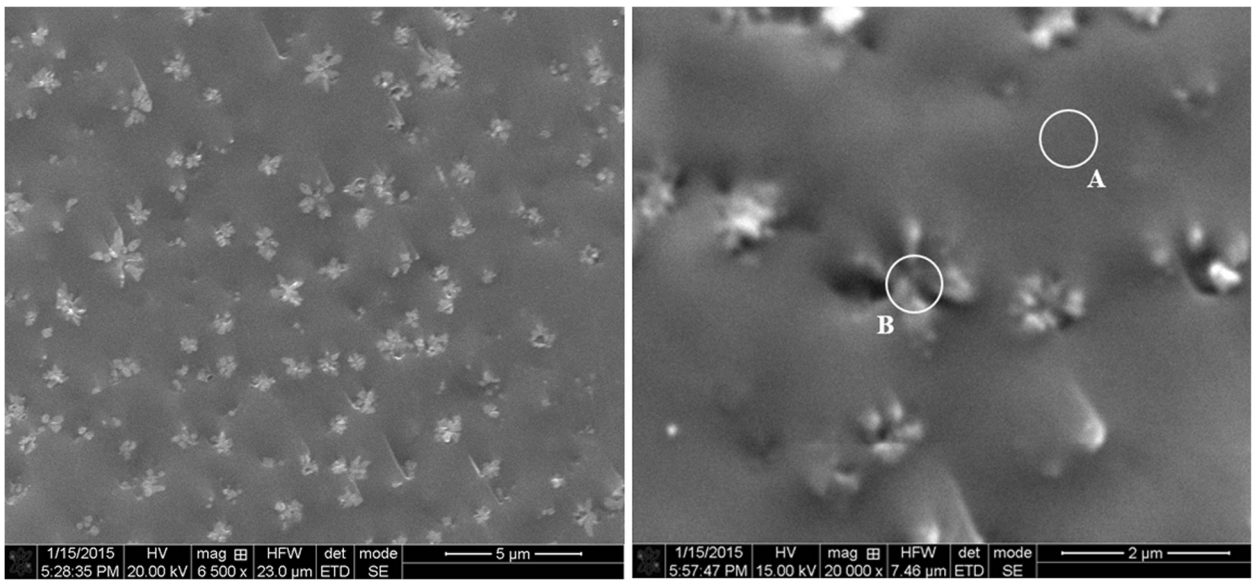

Fig. 2 SEM micrograph of freshly prepared surface cut section of g/c-$Ga_5(As_{0.4}Se_{0.6})_{95}$ alloy, showing regions without visible inclusions (*spot A*) and containing Ga_2Se_3 crystallites (*spot B*)

(each less than 1 μm) being well distinguished at cut surface of g/c-$Ga_5(As_{0.4}Se_{0.6})_{95}$ alloys (Fig. 2). The chemical composition of the sample was checked in two different spots, these being uniform surface area without visible inclusions (A) and one with some agglomerated crystallites (B). The corresponding EDS spectra from these spots detected up to 15 keV (current 0.65 nA) are shown in Fig. 3. Only arsenic As, selenium Se, and gallium Ga were defined as main elements responsible for the observed peaks on these spectra, located respectively to their Lα and Kα states. Despite uncertainties due to large scatter in the experimental points, a sharp increase in Ga and decrease in As content was detected from a crystallite-covered area. In opposite, the uniform sample matrix near crystallites was enriched on As and deficient on Ga, while Se content was nearly the same over a whole sample's surface. These results testify that extraction of Ga_2Se_3 phase is indeed the most plausible reason for growing crystallites.

The above processes essentially modify atomic-deficient void structure of $Ga_x(As_{0.4}Se_{0.6})_{100-x}$ alloys, as it follows from PAL spectra reconstructed within the two-component fitting procedure (Fig. 4) and best-fit positron trapping parameters gathered in Table 1. Since neither average τ_{av} nor defect-free bulk τ_b positron lifetimes are changed under Ga additions, the two-state trapping model based on one preferential type of positron traps [22–26] can be validated as most relevant to the physically realistic channel of positron

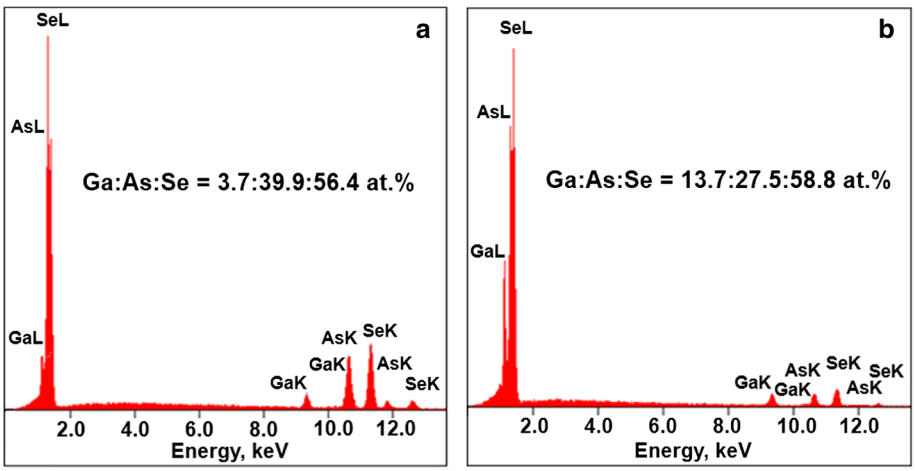

Fig. 3 EDS spectra detected from A (**a**) and B (**b**) spots at the cut surface of g/c-$Ga_5(As_{0.4}Se_{0.6})_{95}$ showing disproportionalities in chemical composition

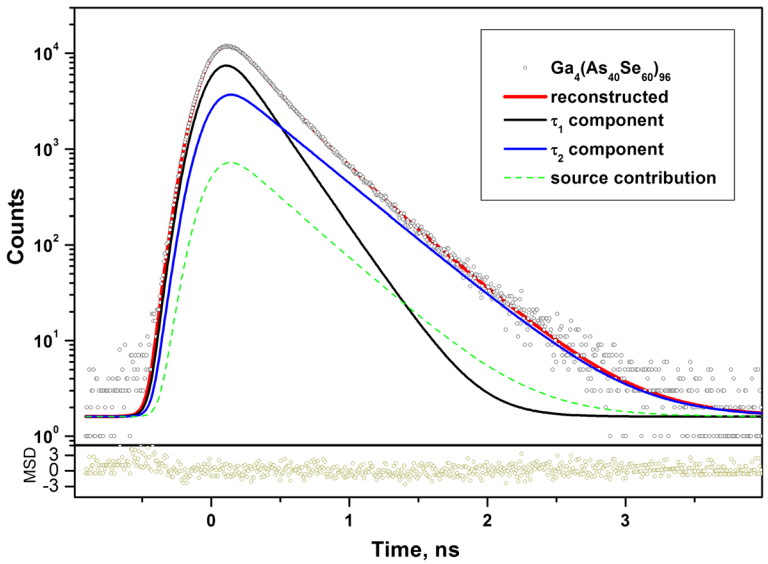

Fig. 4 Raw PAL spectrum of crystallized $Ga_4(As_{0.4}Se_{0.6})_{96}$ alloy reconstructed from a two-component fitting at the general background of source contribution (*bottom inset* shows statistical scatter of variance)

annihilation in these alloys. The volumes of these traps (e.g., sizes of low-electron density spaces) in g or g/c alloys are reflected by defect-related τ_2 lifetimes, while their contents being proportional to intensities of the second fitting components (I_2) [22]. Thus, the positron trapping modes correspondingly recalculated in respect to the above fitting parameters, including trapping rate in defects κ_d, ($\tau_2-\tau_b$) difference, τ_2/τ_b ratio, and fraction of trapped positrons η, can be ascribed to the same type of traps as those characteristic for g-As_2Se_3 [23, 30–33], which are subjected to Ga-activated compositional modification within the $Ga_x(As_{0.4}Se_{0.6})_{100-x}$ system.

In g-As_2Se_3, the positron trapping is defined by spatial distribution of low-electron density spaces (native free-volume voids) formed within *cycle-type* formations of chalcogen-interlinked polyhedrons, such as $AsSe_{3/2}$ pyramids (the fractional subscript means atoms simultaneously belonging to two neighboring units) [23, 31]. Despite deviation in the number of elements forming such cycle-type formations in a glass, they can be considered as network remainders of strict 12-membered cycles in a crystalline structure of rhombohedral As_2Se_3 [34]. In void structure evolution in ChG, an essential role belongs to spaces in the nearest atomic surrounding, which are free of electron density due to directionality of covalent bonds, e.g., bond-free solid angles (BFSA) in terms of Kastner [35]. Depending on electronegativity of neighbors [36], these intrinsic local spaces can be associated with effective neutral (Se atoms in –Se–**Se**–Se– chain- and ring-like fragments), positive (As atoms in the top of $AsSe_{3/2}$ pyramids), or negative (Se atoms within heteronuclear =As–**Se**–As= bridges, e.g., in the bottom of neighboring $AsSe_{3/2}$ pyramids) electrical charge [23, 31, 37]. So the most efficient positron traps in a covalent-bonded network of g-As_2Se_3 represent geometrical free-volume spaces within corresponding cycle-type formations of interlinked

Table 1 Fitting parameters and positron trapping modes describing two-component reconstructed PAL spectra of $Ga_x(As_{0.4}Se_{0.6})_{100-x}$ alloys

Sample, state	Fitting parameters			Positron trapping modes					
	τ_1	τ_2	I_2	τ_{av}	τ_b	κ_d	$\tau_2-\tau_b$	τ_2/τ_b	η
	ns	ns	a.u.	ns	ns	ns^{-1}	ns	–	–
g-As_2Se_3	0.210	0.360	0.462	0.279	0.260	0.92	0.10	1.39	0.19
g-$Ga_1(As_{0.4}Se_{0.6})_{99}$	0.216	0.371	0.408	0.279	0.261	0.78	0.11	1.42	0.17
g-$Ga_2(As_{0.4}Se_{0.6})_{98}$	0.223	0.382	0.401	0.287	0.267	0.75	0.11	1.43	0.17
g-$Ga_3(As_{0.4}Se_{0.6})_{97}$	0.211	0.365	0.457	0.281	0.261	0.91	0.10	1.39	0.19
g/c-$Ga_4(As_{0.4}Se_{0.6})_{96}$	0.204	0.359	0.488	0.280	0.258	1.03	0.10	1.39	0.21
g/c-$Ga_5(As_{0.4}Se_{0.6})_{95}$	0.207	0.362	0.462	0.279	0.258	0.95	0.10	1.40	0.20

$AsSe_{3/2}$ pyramids (atomic-accessible void core) surrounded by low-electron density spaces originated from atomic environment due to strict directionality of covalent chemical bonds (atomic-inaccessible void shell). The possible configurations of some void shells (e.g., BFSA) in ChG systems are considered in more detail elsewhere [23, 37, 38]. If only geometrical free volumes (void cores) have been decisive in a positron trapping in ChG, then defect-related positron lifetime τ_2 would be in strong correlation with molar volume in a g-As–Se system. However, an obviously opposite tendency is observed in g-As–Se, e.g., increase in τ_2 positron lifetime with going from looser Se-rich towards stoichiometric As_2Se_3 and As-rich glasses [31], thus meaning an importance of contribution from agglomerated BFSA (void shells) surrounding geometrical voids. From a standpoint of positron trapping [22], the heteroatomic environment around a chalcogen atom has an obvious preference. Indeed, because of difference in the electronegativity [36], such low-electron density sites carry an effective negative charge, thus transforming corresponding free-volume void in a prototype of cation vacancy in a crystal. This local electrical charge distribution is not characteristic of pure homoatomic Se chains or rings, resulting in reduced positron trapping in Se-rich ChG [31, 32].

In the network of Se-interlinked $AsSe_{3/2}$ pyramids forming the structure of g-As_2Se_3, two of three Se atoms in the bottom of the $AsSe_{3/2}$ pyramid contribute with their BFSA towards free-volume void, while the third Se atom contradicts this because of electron density cone of a covalent bond directed in an opposite hemisphere as void. The geometrically optimized configuration of such $AsSe_{3/2}$ pyramidal cluster computed with ab initio quantum chemical modeling [39] is shown in Fig. 5. Thus, the most expected positron traps in g-As_2Se_3 can be imagined as free-volume voids surrounded by neighboring BFSA originated from two Se atoms (in heteroatomic =As–**Se**–As= environment) of the $AsSe_{3/2}$ pyramid. The expected volumes of such positron traps (near ~90 $Å^3$) can be simply estimated from corresponding defect-related positron lifetime $\tau_2 \cong 0.36$ ns in respect to Jensen's calculations [33]. Possible configuration of such void in orpiment As_2S_3 crystal, the known crystalline counterpart of As_2Se_3 [34], reproduced in respect to electronic structure calculations for mineral arsenic sulfide As_2S_3 performed using Exciting package [40] is depicted in Fig. 6. Undoubtedly, such voids remain in melt-quenched state, thus defining preferential positron trapping in ChG, while voids surrounded by As-based BFSA are rather ineffective for trapping because of repulsive potential for positrons [31, 32]. With transition to over-stoichiometric As-rich ChG, the bridging $As_2Se_{4/2}$ units based on homopolar As–As bonds appear in a network of $AsSe_{3/2}$ pyramids. Both pairs of Se atoms at the edges of the As–As bond contribute fully to free-volume void, since their BFSA are directed to one hemisphere without any restrictions on opposite directionality of Se atoms like in $AsSe_{3/2}$ units (see Fig. 5). So the volumes of such voids grow (in full harmony with decreased atomic densities [34]), thus resulting in enhanced defect-related τ_2 lifetimes for ChG consisting of these structural units, while their concentration (reflected in I_2 intensity) essentially drops in view of chemical formulation [23, 41].

This effect is dominated in g-As_2Se_3 at small Ga addition, specifically in g-$Ga_1(As_{0.4}Se_{0.6})_{99}$ and g-$Ga_2(As_{0.4}Se_{0.6})_{98}$, where increase in τ_2 lifetime from 0.360 to 0.382 ns (Table 1) is caused by transition to positron trapping on free-volume voids neighboring with Se-type BFSA of $As_2Se_{4/2}$ units. The bridging $As_2Se_{4/2}$ clusters appear due to deficit in Se environment for As atoms because of Ga doping at small concentration. Indeed, chemical interaction in a Ga–As–Se system is governed by Ga bonding. By accepting energies for homonuclear Ga–Ga, As–As, and Se–Se bonds as 34.1, 32.1, and 44.0 kcal/mol, respectively [36, 42], the energies for heteronuclear Ga–Se, Ga–As, and As–Se bonds can be estimated in respect to known Pauling's formula [36] as 55.2, 37.2, and 41.7 kcal/mol, respectively. Thereby, the Ga dopants form polyhedra with Se atoms inserted in remainder of the As–Se

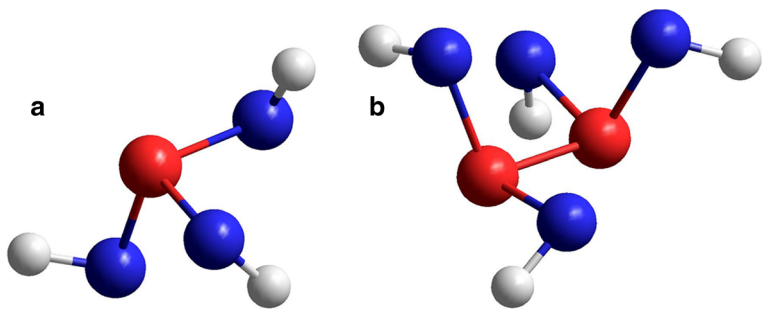

Fig. 5 Geometrically optimized configurations of some atomic clusters in g-As-Se computed by ab initio quantum chemical modeling with RHF/6-311G* basis set [39]. **a** $AsSe_{3/2}$ pyramid (two of three Se atoms contribute with their BFSA to one hemisphere). **b** $As_2Se_{4/2}$ bridge (all four Se atoms contribute with their BFSA to one hemisphere)

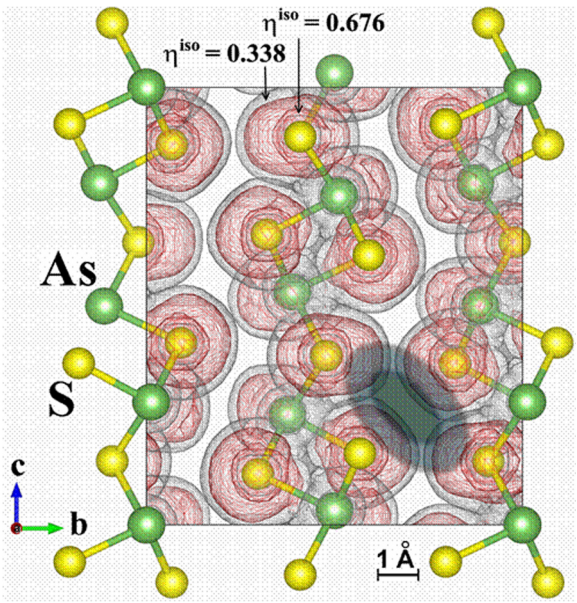

Fig. 6 Electron density distribution in mineral As_2S_3 orpiment visualized with Exciting package [40]: unit cell is along [100] with two isosurface levels of electron localization function (ELF = 0.676, 0.338); the boundaries of free-volume void evolving core and surrounding shell are dark-distinguished

network [8–11, 43, 44]. Because of higher atomic packing of Ga-doped ChG [8–11], this trend is accompanied by reduced second-component I_2 intensity, trapping rate in defects κ_d, and fraction of trapped positrons η in addition to enlarged τ_2 lifetime, $(\tau_2-\tau_b)$ difference, and τ_2/τ_b ratio (Table 1).

Another g-$Ga_3(As_{0.4}Se_{0.6})_{97}$ alloy, possessing positron trapping modes which are rather close to the ones of g-As_2Se_3 (Table 1), is obviously exceptional from the above correlation line. Defect-related annihilation channel in this ChG is presumably distorted due to crystalline nuclei precipitation of separated Ga_2Se_3 phase, like it occurred in $80GeSe_2$–$20Ga_2Se_3$ glass under thermally induced "cold" crystallization [16]. At this stage, the Ga_2Se_3 crystallites do not grow enough to be detected quite reliably with XRPD. The nuclei precipitation process is activated by employing free volume of just attached As-rich matrix with preferential content of bridging $As_2Se_{4/2}$ clusters. Correspondingly, the defect-related τ_2 lifetime drops down to the value of ~0.36 ns, which is characteristic of positron trapping on free-volume voids within $AsSe_{3/2}$-based cycle formations in stoichiometric g-As_2Se_3 (see Table 1).

This process is continued in g/c-$Ga_4(As_{0.4}Se_{0.6})_{96}$ and g/c-$Ga_5(As_{0.4}Se_{0.6})_{95}$ alloys due to further growth and precipitation of Ga_2Se_3 crystallites, which became XRPD-detectable at these conditions (Fig. 1). These crystallites are restricted in their growing in Se-deficient environment, thus being stabilized in the ChG by utilizing atomic-accessible free volumes of their nearest environment rich in $As_2Se_{4/2}$ clusters. In such alloys, the positron trapping on free-volume entities built of pyramidal $AsSe_{3/2}$ units has an obvious preference, tending the overall annihilation-like void fragmentation without notable changes in sizes of positron traps (τ_2 = ~0.36 ns) and enhanced second-component intensities I_2, in full respect to the experimental data in Table 1.

Conclusions

The nanostructurization processes related to evolution of free-volume voids were studied in glassy As_2Se_3 affected by different amounts of Ga additions (up to 5 at. %), using positron annihilation lifetime spectroscopy, the lifetime spectra being analyzed within a canonical two-component model with one preferential type of positron traps. It was shown that below 3 at. % of Ga, when glass formation was not essentially violated, the positron trapping is dominated on intrinsic voids associated with bond-free solid angles of bridging $As_2Se_{4/2}$ units, thus producing an increase in defect-related lifetime from 0.360 to 0.382 ns at the cost of reduced second-component intensity and positron trapping rate in defects. This void agglomeration trend was changed on opposite (void fragmentation) at greater Ga content in As_2Se_3 glass due to crystalline Ga_2Se_3 nuclei precipitation and growth. The observed crystallization processes were activated by employing free volume of just attached As-rich matrix with higher content of $As_2Se_{4/2}$ clusters. In such glassy crystalline alloys, the positron trapping on free-volume entities related to pyramidal $AsSe_{3/2}$ units (as in parent As_2Se_3 glass) was in obvious preference, tending overall annihilation-like void fragmentation without notable changes in sizes of positron traps.

Abbreviations

BFSA: bond-free solid angle; ChG: chalcogenide glass; EDS: energy-dispersive spectroscopy; PAL: positron annihilation lifetime; RE: rare earth; SEM: scanning electron microscope; XRPD: X-ray powder diffraction.

Competing Interests

The authors declare that they have no competing interests.

Authors' Contributions

All authors (YaSh, AI, OSh, AD, CB, BB) developed the methodological algorithms to treat experimental PAL spectra. AI and YaSh performed the experiments to characterize the samples. YaSh, CB, and BB prepared the tested objects. AD and ShYa performed the SEM and EDS analyses. All authors read and approved the final manuscript.

Acknowledgements

This research is supported by POLONIUM common actions program for years 2015–2016 realized in respect to bilateral agreement on scientific-technical cooperation between Polish and French governments from 1966. Support from Marie-Curie Action FP7-PEOPLE-2010-ITN under the GlaCERCo project is also acknowledged.

Author details

[1]Department of Electronics, Ivan Franko National University of Lviv, 107, Tarnavskogo str., 79017 Lviv, Ukraine. [2]Centre for Innovation and Transfer of Natural Sciences and Engineering Knowledge, University of Rzeszow, 1, Pigonia str., 35-959 Rzeszow, Poland. [3]Laboratoire Verres et Céramiques, UMR-CNRS 6226, Université de Rennes 1, 35042 Rennes, Cedex, France.

[4]Opole University of Technology, 75, Ozimska str., 45370 Opole, Poland.
[5]Vlokh Institute of Physical Optics, 23, Dragomanov str., 79005 Lviv, Ukraine.
[6]Institute of Physics, Jan Dlugosz University, 13/15, Armii Krajowej al., 42200 Czestochowa, Poland.

Received: 26 October 2015 Accepted: 5 January 2016
Published online: 13 January 2016

References

1. Cole B, Shaw LB, Pureza PC, Mossadegh R, Sanghera JS, Aggarwal ID (1999) Rare-earth doped selenide glasses and fibers for active applications in the near and mid-IR. J Non-Cryst Solids 256–257:253–259
2. Lezal D (2003) Chalcogenide glasses. J Optoelectron Adv Mater 5:23–34
3. Choi YG (2007) Spatial distribution of rare-earth ions in Se-based chalcogenide glasses with or without Ga. J Non-Cryst Solids 353(18–21): 1930–1935
4. Seddon AB, Tang Z, Furniss D, Sujecki S, Benson TM (2010) Progress in rare earth-doped mid-infrared fiber lasers. Opt Express 18(25):26704–26719
5. Charpentier F, Starecki F, Doualan JL, Jóvári P, Camy P, Troles J, Belin S, Bureau B, Nazabal V (2013) Mid-IR luminescence of Dy^{3+} and Pr^{3+} doped $Ga_5Ge_{20}Sb_{10}S(Se)_{65}$ bulk glasses and fibers. Mater Lett 101:21–24
6. Starecki F, Charpentier F, Doualan JL, Quetel L, Michel K, Chahal R, Troles J, Bureau B, Braud A, Camy P, Moizan V, Nazabal V (2015) Mid-IR optical sensor for CO_2 detection based on fluorescence absorbance of Dy^{3+}:$Ga_5Ge_{20}Sb_{10}S_{65}$ fibers. Sens Actuators, B 207:518–525
7. Pelé AL, Braud A, Doualan JL, Chahal R, Nazabal V, Boussard-Plédel C, Bureau B, Moncorgé R, Camy P (2015) Wavelength conversion in Er^{3+} doped chalcogenide fibers for optical gas sensors. Opt Express 23(4):4163–4172
8. Ya S, Bureau B, Boussard C, Nazabal V, Golovchak R, Demchenko P, Polovynko I (2014) Effect of Ga incorporation in the $As_{30}Se_{50}Te_{20}$ glass. J Non-Cryst Solids 398–399:19–25
9. Ya S, Boussard-Pledel C, Nazabal V, Chahal R, Ari J, Pavlyk B, Cebulski J, Doualan JL, Bureau B (2015) Ga-modified As_2Se_3-Te glasses for active applications in IR photonics. Opt Mater 46:228–232
10. Golovchak R, Shpotyuk Y, Nazabal V, Boussard-Pledel C, Bureau B, Cebulski J, Jain H (2015) Study of Ga incorporation in glassy arsenic selenides by high-resolution XPS and EXAFS. J Chem Phys 142(18):184501-1-10
11. Golovchak R, Shpotyuk Y, Thomas CM, Nazabal V, Boussard-Pledel C, Bureau B, Jain H (2015) Peculiarities of Ga and Te incorporation in glassy arsenic selenides. J Non-Cryst Solids 429:104–111
12. Liu C, Tang G, Luo L, Chen W (2009) Phase separation inducing controlled crystallization of $GeSe_2$-Ga_2Se_3-CsCl glasses for fabricating infrared transmitting glass-ceramics. J Am Ceram Soc 92(1):245–248
13. Shpotyuk O, Ingram A, Bureau B, Shpotyuk Y, Boussard C, Nazabal V, Szatanik R (2014) Positron annihilation probing of crystallization effects in TAS-235 glass affected by Ga additions. J Phys Chem Solids 75(9):1049–1053
14. Roze M, Calvez L, Ledemi Y, Allix M, Matzen G, Zhang X (2008) Optical and mechanical properties of glasses and glass–ceramics based on the Ge–Ga–Se system. J Amer Ceram Soc 91(11):3566–3570
15. Golovchak R, Calvez L, Petracovschi E, Bureau B, Savytskii D, Jain H (2013) Incorporation of Ga into the structure of Ge-Se. Mater Chem Phys 138:909–916
16. Shpotyuk O, Calvez L, Petracovschi E, Klym H, Ingram A, Demchenko P (2014) Thermally-induced crystallization behaviour of $80GeSe_2$-$20Ga_2Se_3$ glass as probed by combined X-ray diffraction and PAL spectroscopy. J Alloys Compd 582:323–327
17. Hubert M, Delaizir G, Monnier J, Godart C, Ma H, Zhang X, Calvez L (2011) An innovative approach to develop highly performant chalcogenide glasses and glass-ceramics transparent in the infrared range. Opt Express 19(23): 23513–23522
18. Cui S, Chahal R, Shpotyuk Ya, Boussard-Pledel C, Lucas J, Charpentier F, Tariel H, Loreal O, Nazabal V, Sire O, Monbet V, Yang Z, Lucas P, Bureau B (2014) Selenide and telluride glasses for mid-infrared bio-sensing. Proc SPIE 8938:893805-1-9.
19. Eggleton BJ, Luther-Davies B, Richardson K (2011) Chalcogenide photonics. Nat Photonics 5:141–148
20. Rodriguez-Carvajal J (2001) Recent developments of the program FullProf. Commission on Powder Diffraction Newsletters 26:12–19
21. Kansy J (1996) Microcomputer program for analysis of positron annihilation lifetime spectra. Nucl Instrum Methods Phys Res, Sect A 374(2):235–244
22. Krause-Rehberg R, Leipner H (1999) Positron annihilation in semiconductors: defect studies. Springer, Heidelberg
23. Shpotyuk O, Filipecki J (2003) Free volume in vitreous chalcogenide semiconductors: possibilities of positron annihilation lifetime study. WSP, Czestochowa
24. Keeble DJ, Brossmann U, Puff W, Würschum R (2012) Positron annihilation studies of materials. In: Kaufmann EN (ed) Characterization of materials. John Wiley & Sons, Inc., New York, pp 1899–1925
25. Tuomisto F, Makkonen I (2013) Defect identification in semiconductors with positron annihilation: experiment and theory. Rev Mod Phys 85:1583–1631
26. Seeger A (1974) The study of defects in crystals by positron annihilation. Appl Phys 4(3):183–199
27. Khan MY, Ali SZ (1980) Optical and scanning electron microscopic examination of α- and β-Ga_2Se_3. J Cryst Growth 49(2):303–308
28. Ali SZ, Khan MY (1981) Duplex character of defect zinc blende structure of α- and γ-Ga_2Se_3. Acta Cryst 37:C104b
29. Massalski TB, Okamoto H, Subramanian PR, Kacprzak L (1990) Binary alloy phase diagrams, 2nd edn. ASM International, Materials Park, OH
30. Hyla M, Filipecki J, Shpotyuk O, Popescu M, Balitska V (2007) Stoichiometric arsenic sulphoselenides as testing probes for positron trapping in chalcogenide glasses. J Optoelectron Adv Mat 9:3177–3181
31. Ingram A, Golovchak R, Kostrzewa M, Wacke S, Shpotyuk M, Shpotyuk O (2012) Compositional dependences of average positron lifetime in binary As-S/Se glasses. Physica B 407(4):652–655
32. Shpotyuk O, Golovchak R, Ingram A, Boyko V, Shpotyuk L (2013) Comparative study of extended free-volume defects in As- and Ge-based glassy semiconductors: theoretical prediction and experimental probing with PAL technique. Phys Status Solidi C 10(1):117–120
33. Jensen KO, Salmon PS, Penfold IT, Coleman PG (1994) Microvoids in chalcogenide glasses studied by positron annihilation. J Non-Cryst Solids 170(1):57–64
34. Feltz A (1993) Amorphous inorganic materials and glasses. VCH Publishers, New York
35. Kastner M (1973) Compositional trends in the optical properties of amorphous lone-pair semiconductors. Phys Rev B 7(12):5237–5252
36. Pauling L (1960) The nature of the chemical bond. Cornell Univ. Press, Ithaca
37. Shpotyuk OI, Filipecki J, Balitska VO (2008) Radiation-induced extended free-volume defects in mixed ternary Ge-As/Sb-S glasses studied with PALS technique. J Optoelectron Adv Mat 10:3193–3197
38. Shpotyuk O, Ingram A, Demchenko P (2015) Free volume structure of realgar α-As_4S_4 by positron annihilation lifetime spectroscopy. J Phys Chem Solids 79:49–54
39. Shpotyuk O, Hyla M, Boyko V (2015) Compositionally-dependent structural variations in glassy chalcogenides: the case of binary As-Se system. Comput Meter Sci 110:144–151
40. Exciting Beryllium, program package. 2013. http://exciting-code.org. Accessed 25 Sept 2015.
41. Alekseeva OK, Mikhailov VI, Shantarovich VP (1978) Positron annihilation in point defects of the glassy As-Se system. Phys Status Solidi A 48:K169–K173
42. Tichy L, Ticha H (1995) Covalent bond approach to the glass-transition temperature of chalcogenide glass. J Non-Cryst Solids 189:141–146
43. Aitken BG, Ponader CW, Quimby RS (2002) Clustering of rare earths in GeAs sulfide glass. C R Chimie 5(12):865–872
44. Churbanov MF, Scripachev IV, Shiryaev VS, Plotnichenko VG, Smetanin SV, Kryukova EB, Pyrkov YN, Galagan BI (2013) Chalcogenide glasses doped with Tb, Dy and Pr ions. J Non-Cryst Solids 326–327:301–305